Predicting Observing Conditions at ESO Observatories – Reality and Perspectives*

M. SARAZIN, ESO

1. Introduction

It is now understood that most future ground-based observatories will make use of flexible scheduling tools to select the observing mode best adapted to the observing conditions.

ESO has been conducting a wide survey of existing and potential forecasting techniques and, on the basis of a strategy described in Figure 1, several feasibility studies were initiated from 1992 onwards, both internally and externally. Most of them are completed or close to completion. It is thus time to prepare the specifications of the operational tools and services to be developed for the VLT.

For this purpose, a workshop on *Forecasting Astronomical Observing Conditions* took place on 29–30 May, 1997 at ESO Garching. A summary of the main results is presented in what follows, trying to establish the current state of the art applicable to Chilean observatories as a whole.

In his introductory talk, the ESO Director General stressed that ESO is aiming at the highest observing efficiency at the VLT to make possible the scientific discoveries the astronomical community legitimately expects from such a tool. The DG also indicated that the cost of a night of operation of the observatory (≈ 100,000 DM) gives the scale for deciding the extent to which ESO should push research in modelling and prediction. He noted in particular that he would probably exclude launching a dedicated satellite (as proposed by one of the speakers) but that he would certainly support further measurement campaigns or local instrumentation development if deemed necessary.

In what follows, the meteorologists attempt to answer questions preoccupying most individuals involved in the planning of observatory operation. A common tool for all studies is the invaluable forecast service provided by ECMWF (European Centre for Medium-Range Weather Forecasts) or its US equivalent NCEP (National Centre for Environmental Prediction). We are grateful to ECMWF to have accepted ESO's invitation to be represented at this workshop to introduce the participants to the complex world of forecasting.

2. Forecasting Cloudiness and Water Vapour

Will next night be photometric? When to schedule infrared observing? How stable is the current situation?

2.1 Meteorology and satellite images

The study of ECMWF forecast skill over ESO observatories ([CRS4 97]) has shown that the global forecasts of cloudiness and water vapour did not reach the type of accuracy needed for astronomy. A more successful method proposed by [Erasmus 97] combines synoptic scale circulation modelling with ECMWF standard forecasts and analyses (geopotential height, wind components, temperature and vertical velocity) as well as local surface relative humidity to extract from a 6.7 μm satellite image, the pixels which will pass over the observatory during the period predicted, and the corresponding water vapour content. The large-scale circulation patterns affecting the Chilean coast are presented in Figure 2. The particular situation of the Atacama desert with respect to cloudiness and water vapour is clearly illustrated. Here follows a summary of the presentation by A. Erasmus:

In summer the pressure systems move southwards and the Subtropical high pressure (H) strengthens and expands its area of influence. Subsidence in the high creates a strong temperature inversion at about 1000 m above the surface which traps low-level stratocumulus clouds below it (notice the area of medium grey speckled cloud in and around the high). The subtropical high is a semi-permanent circulation feature that only experiences minor position changes as the high develops east or west of its mean position. The high produces clear dry conditions over northern Chile. Occasional incursions of moisture and cloud may occur over northern Chile from the north in summer if the high weakens and the anticyclonic flow over the Amazon basin intensifies.

In winter the pressure systems move northwards and the subtropics comes under the influence of migratory wave-like systems that propagate from west to east in the prevailing flow. The high pressure area of the wave (the ridge) is warm and dry while the low pressure area (the trough) is cool and moist. Middle and upper tropospheric clouds can typically be found along the leading edge of the ridge and trough in association with surface warm and cold fronts. Trough and ridge development, which is

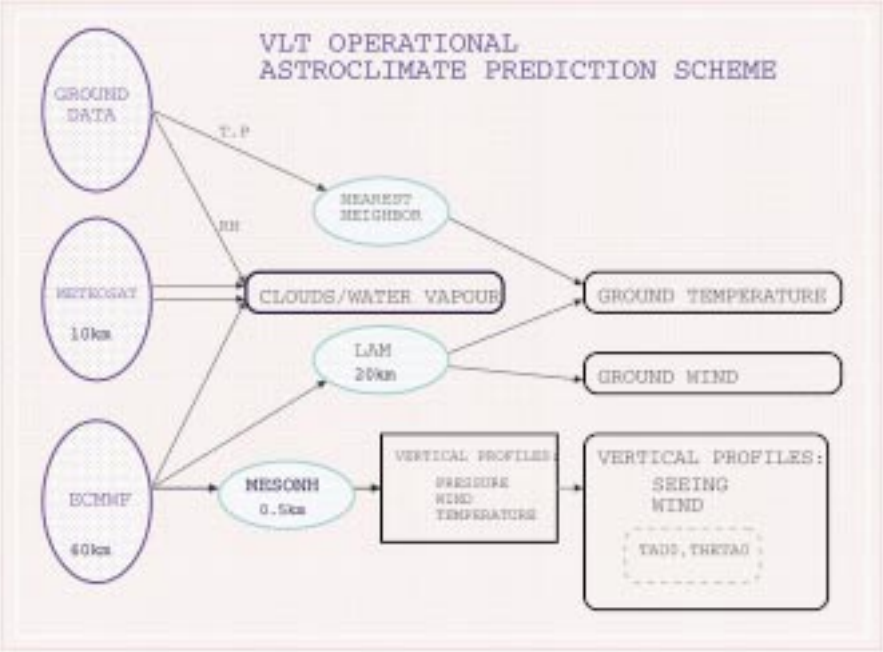

Figure 1: Initial organigram of the prediction strategy for the VLT Observatory.

*This article summarises the talks and discussions during the meeting. Speakers were A. Erasmus (University of Northern Colorado), A. Speranza, R. Deidda and M. Maroccu (CRS4, Cagliari), J. Vernin and E. Masciadri (University of Nice), A. Lanzinger (ECMWF Reading) and the author of the present article. The agenda of the Workshop can be found in *The Messenger* No. 88, June 1997, p. 35.

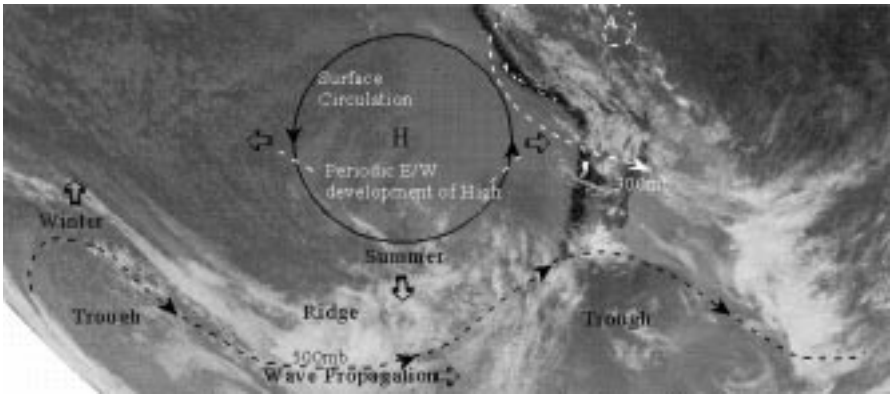

Figure 2: Schematic diagram showing the main synoptic scale circulation systems that control water vapour and cirrus cloud cover advection patterns over the South-eastern Pacific Ocean. The satellite image is taken at 11 μm in the atmospheric IR window. Warmer surfaces appear dark and cold surfaces light. Clouds behave essentially as blackbodies at this wavelength, hence low clouds (being warmer) are medium grey and higher clouds (being cold) appear light grey or even white for the highest (about 15 km), coldest cirrus clouds.

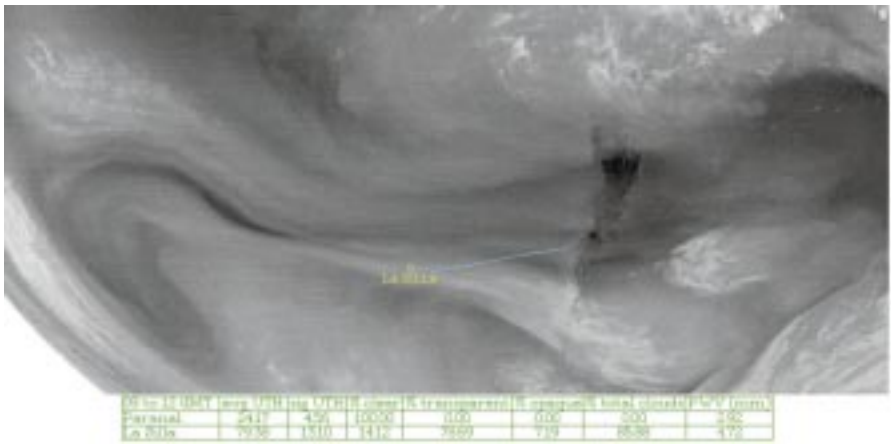

Figure 3: Sample 6.7 μm Satellite Image and Output of Cloudiness and Water Vapour Forecast over La Silla Observatory: the model identifies at 15 h UT, on November 29, 1993, the image pixel which will most probably pass over the observatory 20 hours later.

usually slight over the south-eastern Pacific, may add a meridional component to the cloud cover and water vapour advection patterns.

2.2 Forecast skill

It was demonstrated that operational forecast of cloudiness and water vapour is feasible for observatories in Chile. The product illustrated in Figure 3 consists of a daily estimate of the percentage of the sky to be clear, covered with transparent cirruses, or by opaque clouds, and the total amount of precipitable water vapour, for the next 24 hours by periods of 3 hours. In addition, an up to 7-day daily outlook of status and tendency will be issued on qualitative grounds such as dry/moist and persisting/drying/moistening.

The image area trajectory is forecast with an rms error below 8% in image transparency units. The water vapour forecasts agree with infrared radiometric measurements taken from the ground at Paranal (NOAO Water Vapour Monitor) within an rms of 1.0 mm H_2O (comparable to the dispersion between the WVM ground measurements and the Antofagasta radiosonde). Cloudy sky is successfully forecast 95% of the time at Paranal and 84% at La Silla, with respectively 2% and 7% false alarm rate.

3. Forecasting Temperature and Wind at Ground Level

3.1 24-hour ahead temperature forecasts

At which temperature should the air conditioning of the enclosure be preset during the day so that the telescope and primary mirror are in thermal equilibrium with the outside air at the beginning of the next night?

A chronologically first, non meteorological approach was to train some statistical engine on the large database available for ESO sites. An internal study was conducted ([Aussem 94]) and led to the results presented in Table 1 where the nearest neighbour technique clearly outperforms the neural nets, in particular with regard to the fine tuning of the forecast (prediction error smaller than 0.5 Celsius in 62% of the cases). However, as could be expected, none of these techniques can catch weather trends leading to abrupt temperature shifts of 2 to 6 degrees in 24 hour, representing about 15% of the time at Paranal during the season studied (summer).

Could large ΔT be better predicted using meteorological models? Obviously, a global model such as ECMWF has a mesh much too large (ca. 60 km) for the steep terrain surrounding astronomical sites. Such a model has to be complemented either by a statistical post-processing such as Kalman filtering, or by a local area model (LAM) implementation. The study of 4 sample years conducted by [CRS4 97] concluded that the poorness of local measurements over the Pacific was limiting the accuracy of ECMWF forecasts on the Chilean coast. A LAM initialised by erroneous forecasts without injection of additional observational data could obviously not improve the detection of unpredicted weather changes coming from outside its orographic limits.

Table 2 shows however that a simple Kalman postprocessing of ECMWF 24-hour forecasts successfully cancels the forecast systematic errors (the correlation coefficient of postprocessed forecasts is as good as for the analysis). As expected, postprocessing alone is not able to remove synoptic errors so that large differences between actual and forecasted temperatures still subsist. Table 3 summarises the forecast skill at 12 hour UT at Paranal as a function of 24-hour temperature changes, it shows that 55% – (159+158)/572 – versus 40% – (112+117)/572 – of the cases are brought inside the ±1 C range, and that 84% versus 69% are smaller than ±2 C. These performances are very similar to the results obtained with the statistical method of Table 1, however it is believed – but not proven – that the cases corrected by either methods have little in common, so that a mixture of both techniques (as proposed on Fig. 1) would consistently improve the forecast skill.

Prediction error (Celsius)	≤ 2	≤ 1	≤ 0.5
Best Nearest Neighbour	84%	73%	62%
Best Neural Network	71%	43%	22%
Carbon Copy $t_n = t_{n-1}$	63%	36%	19%

Table 1: 24-hour ahead statistical forecast of ground temperature at each hour of the day: hit rate of nearest neighbour and neural network methods over 18,000 observations corresponding to summer 1989/1990 at Paranal. Nearest neighbour predictions were carried out on a 5-tupple set of the type [t_{n-1}, t_{n-2}, t_{n-3}, p_{n-1}, p_{n-2}].

Site	N	$\lvert\varepsilon^{Kal}\rvert$	r^{Kal}	$\lvert\varepsilon^{per}\rvert$	r^{per}	r^{for}	r^{ana}
La Silla	1114	1.6	0.86	2.1	0.77	0.82	0.86
Paranal	572	1.1	0.88	1.5	0.80	0.79	0.87

Table 2: Absolute mean errors ($\lvert\varepsilon\rvert$) and correlations (r) between observed 2-metre temperatures (C) and estimations by Kalman filter post-processing (^{Kal}) compared to persistence (^{per}), ECMWF 24-hour forecast (^{for}), and ECMWF analysis (^{ana}). N is number of data used for comparison during the period from 1989 to 1993.

Let us extract from Table 3 the forecast skill in the cases when the telescope temperature would be 2 C or more warmer than the outside air, a situation which is detrimental for observations at all wavelengths (local seeing greater than 1 arcsec in the visible). Such cases are down by a factor of 2 from 15% –(4+11+22+46)/572 – to 7.5% –(2+3+12+33)/572). Converting the overall temperature unbalance of Table 3 into mirror seeing with a rate of 0.5 arcsec per positive degree and 0.1 arcsec per negative degree, we obtain a yearly average mirror seeing in the first hour of observation of 0.48 arcsec with persistence ($T_n = T_{n-1}$) down to 0.35 arcsec when Kalman filtered ECMWF forecasts are used.

3.2 24-hour-ahead forecasts of wind 10 metres above ground

Is there any chance that observations have to be stopped in the course of the night because the wind is reaching the maximum operating velocity (20 m/s)?

This topic did not meet a satisfying answer until now. The results of Table 4 by [CRS4 97] show large errors and poor correlation of 10-metre wind forecasts and analyses with data measured at Paranal or La Silla.

As for 2-metre temperature, much of ECMWF forecast error is due to the lack of observational data in the Antofagasta area and could not be corrected by implementing a LAM (20 km mesh) without injection of new observational data. However, unlike 2-metre temperature, not only the forecasts but also the analyses are poorly correlated. Obviously, a global model such as ECMWF and even the LAM have a mesh much too large for the steep terrain surrounding astronomical sites. One has probably to go down to a mesoscale model such as the one described in Section 4.2 (ca. 500 m mesh). A sample output on Figure 4 shows that local overspeed and shears are then clearly visible. Other more straightforward methods such a modified mass-consistency models could be investigated to improve the case of 10-metre wind forecast.

4. Forecasting Seeing

4.1 Introduction

Does it make sense to plan using adaptive optics in the next coming hours? What is the improvement in Strehl ratio to be expected?

To answer this question, two parameters have to be known: the distribution of the turbulence along the path, and its rate of change. The strategy chosen to obtain such forecasts requires three steps:

(1) Obtain a reliable forecast of the vertical profile of the temperature of the atmosphere several tens of kilometres upwind (Section 4.3).

(2) Use this profile to initialise a mesoscale model capable to reflect the effect of the terrain on an unperturbed atmosphere, in particular the triggering of gravity waves or the increase of mixing due to orographic wind shear (Section 4.2).

(3) Combine the output of the mesoscale model (vertical profile of turbulence corresponding to the forecasted vertical profile of temperature) with a forecast of the vertical profile of the wind field above the observatory so as to compute the wavefront velocity (Section 4.4).

Actual 24-hour change (*K*)

KFPP Error (*K*)	–6	–5	–4	–3	–2	–1	1	2	3	4	5	6	KFPP Scores
–6	0	0	0	1	1	0	0	0	0	0	0	0	2
–5	0	0	0	0	0	0	0	0	0	0	0	0	0
–4	0	1	1	4	2	1	0	0	0	0	0	1	10
–3	0	1	3	8	9	3	3	2	1	1	0	0	31
–2	1	2	11	14	17	22	9	3	0	0	0	0	79
–1	1	5	3	14	38	38	34	15	9	2	0	0	159
1	2	2	2	4	15	34	47	28	16	5	3	0	158
2	0	0	2	1	5	9	21	15	18	5	5	2	83
3	0	0	0	0	4	5	2	6	10	1	2	3	33
4	0	0	0	0	0	0	1	3	4	2	1	1	12
5	0	0	0	0	0	0	0	1	0	1	1	0	3
6	0	0	0	0	0	0	0	0	1	0	0	1	2
	4	11	22	46	91	112	117	73	59	17	12	8	

Global scores of persistence

Table 3: Contingency table between errors of Kalman Filtering Postprocessing Procedure (KFPP) and Air Temperature (T_{2m}) daily variation at Paranal during the period 1989–1993 at 12GMT. Sum of the counts along rows (shown in the last column of the table) is the number of times T_{2m} has been forecasted within an error indicated in the first column of the table itself. Sum of the numbers along a column (shown in the last row), is the number of times T_{2m} has had a diurnal variation within the value shown in the first row. The generic count within a cell of the table gives number of times T_{2m} has been forecasted within an error indicated in the corresponding cell of the first columns when the daily variation of T_{2m} was that indicated in the corresponding cell of the last row.

Site	N	$\lvert\varepsilon^{Kal}\rvert$	r^{Kal}	$\lvert\varepsilon^{per}\rvert$	r^{per}	r^{for}	r^{ana}
La Silla	1242	2.5	0.64	2.9	0.59	0.57	0.43
Paranal	608	3.0	0.59	3.4	0.56	0.50	0.64

Table 4: Absolute mean errors ($\lvert\varepsilon\rvert$) and correlations (r) between observed 10-metre wind speed (m/s) and estimations by Kalman Filtering Postprocessing Procedure or KFPP (^{Kal}) compared to persistence (^{per}), ECMWF 24-hour forecast (^{for}), and ECMWF analysis (^{ana}). N is number of data used for comparison during the period from 1989 to 1993.

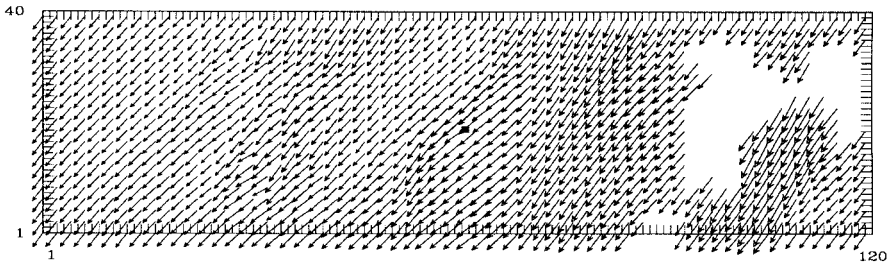

Figure 4: Sample Output of Surface Wind Mesoscale Modelling in the Paranal Area at 2600 m altitude on the terrain model of Figure 5 [Masciadri 97].

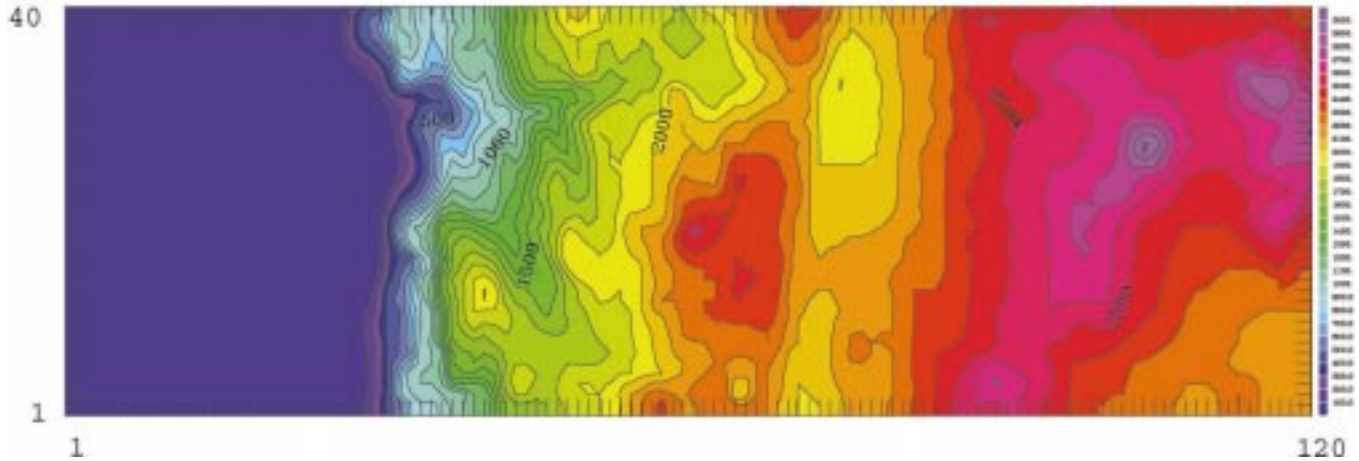

Figure 5: Input terrain model for Mesoscale Modelling in the Paranal Area with a 500 m horizontal resolution over an area of 60 × 20 km centred on the site.

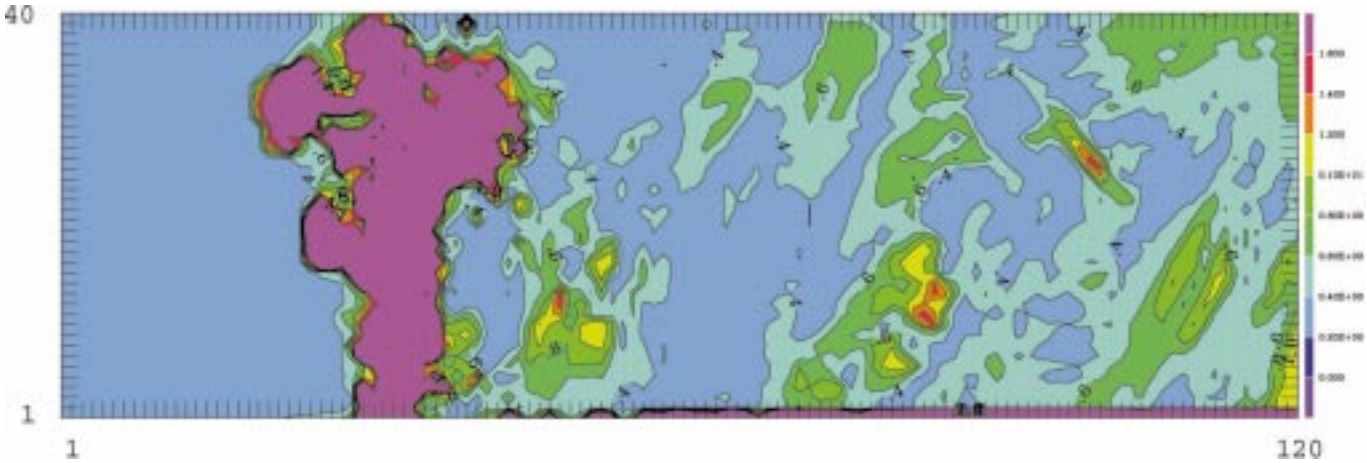

Figure 6: Sample Output of Seeing Mesoscale Modelling in the Paranal Area with the terrain model of Figure 5, colour scale is arbitrary, in units of FWHM (arcsec). The steep coastal slopes appear to strongly perturbate the optical steadyness of the airflow from the Pacific.

4.2 Modelling seeing

Following earlier attempts by [Bougeault 95] of a mesoscale model applied on a mountainous continental site, a feasibility study has been started by [Masciadri 97] for the Paranal area using the recently developed non-hydrostatic model, meso-nh, including slight modifications appropriate to optical turbulence modelling. The model is non-hydrostatic, and as such allows the vertical development of orographic waves which are believed to be responsible of a large part of the night-time tropospheric seeing. Such waves indeed create areas with high kinetic energy (and thus well mixed air) at the boarder of which strong vertical gradients of the potential temperature constitute *sheets* of high optical turbulence.

One of the possible outputs of such a 3-D model shown in Figure 6, could obviously be useful during site surveys to exclude potentially unfavourable areas such as the immediate vicinity of the steep coastal slopes.

Tuning a model such as meso-nh is a complicated task because two parameters have to be minimised: the modelling error and the operational cost. Table 5 clearly illustrates the challenge. The cheapest configuration would allow several runs per night to be performed in an operational manner, while the two highest costs would simply forbid any operational use. Initial results of the study by [Masciadri 97] show that a simulated time of 30 minutes is often not sufficient to fully resolve terrain-atmosphere interaction, it is thus reasonable to assume that the cost of a simulation will be of the order of a few hundred DM.

4.3 Forecasting wavefront isoplanaticity

Assuming the decision is made to use adaptive optics, how far away from the line of sight can a natural guide star be chosen? In case no convenient natural guide star is available for a given scientific object, will the cone effect be small enough to allow laser-guide-star operation?

The answers depend on the relative vertical distribution of the turbulence expected above the observatory, expressed as an isoplanatic angle θ_0:

$$\theta_0 = [\int C_n^2(h) h^{5/3} dh]^{-3/5} \qquad (1)$$

Let us assume that it is possible to model the vertical distribution of the index of refraction structure coefficient (C_n^2)with an input vertical profile of tem-

Area (km	Vert. Res. (m)	Horiz. Res. (m)	Simulated Time (sec)	Time Step (sec)	CPU Time (sec)	Price (DM)
60 × 20	300	500 × 500	1800	2.5	4629	1388
60 × 20	600	500 × 500	1800	2.5	1945	583
60 × 20	300	1000 × 1000	1800	5	719	215
60 × 20	600	1000 × 1000	1800	5	296	88
60 × 60	300	500 × 500	1800	2.5	13219	3965
120 × 120	600	2000 × 2000	1800	10	400	120

Table 5: According to the configuration chosen, the cost of a prediction (based on 1997 CRAY90 CPU charges) can vary by a factor of 50.

		1993			1989–1993
Site & hour	ECMWF	corr	err	| err |	| err |
Antofagasta 12GMT	Analysis	0.986	1.39	2.54	2.50
	24h For.	0.985	1.41	3.00	2.91
	48h For.	0.984	1.32	3.24	3.11
Quintero 12GMT	Analysis	0.991	1.15	2.48	2.52
	24h For.	0.989	1.35	3.39	3.25
	48h For.	0.988	1.37	3.96	3.71

Table 6: Averages of daily correlations, mean errors, and mean absolute errors of radio sounding temperatures against ECMWF analysis and 24/48-hour forecast during 1993 period and during the 1989–1993 period.

			m/s	
Site & hour	ECMWF	corr	err	| err |
Antofagasta 12GMT	Analysis	0.918	–0.36	2.11
	24h For.	0.813	–3.36	4.31
	48h For.	0.781	–0.24	5.09
Quintero 12GMT	Analysis	0.854	1.04	4.26
	24h For.	0.785	0.95	6.13
	48h For.	0.748	1.05	7.24

Table 7: Averages of daily correlations, mean errors, and mean absolute errors of radio sounding wind velocity against ECMWF analysis and 24/48-hour forecast during the 1993 period. The larger error at Quintero in 1993 is due to the blacklisting of this station from the ECMWF data assimilation scheme.

	Antofagasta		Quintero	
	1993	1989–1993	1993	1989–1993
Analysis	20%	21%	52%	31%
24h For.	48%	46%	98%	62%
48h For.	63%	58%	118%	80%

Table 8: Averages of daily relative unsigned errors of radio sounding wind velocity against ECMWF analysis and 24/48-hour forecast during 1993 period and during the 1989–1993 period. The larger error at Quintero in 1993 is due to the blacklisting of this station from the ECMWF data assimilation scheme.

perature measured locally by a radiosonde as described in Section 4.2. Could the radiosonde measurement be replaced by a forecasted temperature profile to obtain from meso-nh a forecast of the vertical profile $C_n^2(h)$ above Paranal?

According to the conclusion of the evaluation of ECMWF forecast skill by [CRS4 97], summarised in Table 6, the temperature profile is accurately represented and correctly forecast at the two Chilean radiosonde launching sites. The question was raised if a profile obtained under the hydrostatic assumption could be used to initialise a non-hydrostatic model such as meso-nh. It was answered that although this would normally not be possible, the particular case of the Chilean coast was allowing this approximation: the general motion being eastwards, air masses are reaching the coast undisturbed by orography. The verification of this assumption is the object of the next phase of the study by [Masciadri 97], comparing model results to actual C_n^2 profiles measured from Paranal with balloon borne microthermal probes and by the SCIDAR technique.

4.4 Forecasting Wavefront Temporal Characteristics

Will the adaptive optics system be fast enough to follow the wavefront temporal evolution?

The atmospheric seeing, expressed as the Full Width at Half Maximum (FWHM) of a long-exposure image at an aberration-free telescope (FWHM $\approx \lambda / r_0$) *is* the cumulative effect of numerous *sheets* of refractive index perturbations all the way from about 20 km altitude down to the telescope enclosure (dome, mirror and instrument seeing are excluded from this section). Each turbulence sheet at altitude h has its own $r_0(h)$ and moves with the wind at a velocity $\upsilon(h)$ in the direction $\theta(h)$. If each sheet bears a fraction $\alpha(h)$ of the total turbulence (as r_0 varies as the –3/5 power of the turbulence, we have $\alpha(h) = [\frac{r_0}{r_0(h)}]^{\frac{5}{3}}$), the resultant wavefront corrugations horizontal velocity at ground level is

$$V_0 = [\sum \alpha(h) \vec{\upsilon}(h)^{\frac{5}{3}}]^{\frac{3}{5}} \qquad (2)$$

and the coherence time will be proportional to the time needed for the wavefront to move by one coherence cell:

$$\tau_0 \approx 0.3 \frac{r_0}{V_0} \qquad (3)$$

It is thus clear from Figure 7 that for a given seeing vertical distribution V_0 will be much larger – and τ_0 much smaller – during austral winter. Moreover, 24-hour ECMWF predictions of wind velocity

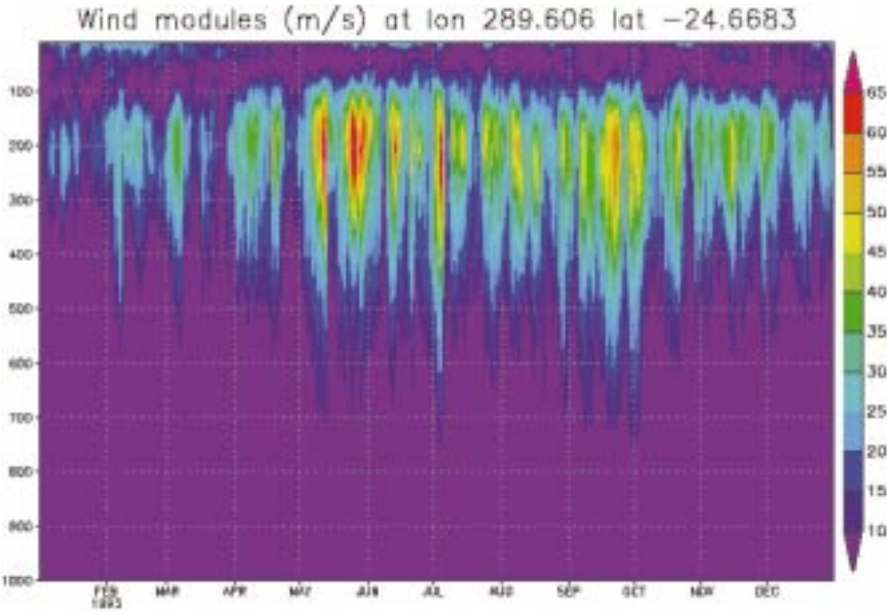

Figure 7: ECMWF wind velocity vertical profiles above Paranal: the period May to October is characteristic of potential jet stream development at 200 mB. The effect of high altitude wind is also noticeable down to the level of the VLT site (740 mB).

would as such, even with the 46% error displayed in Table 8, allow to classify the next night as potentially slow or rapid. Finally, considering the rather high correlation coefficients given in Table 7, it is believed that a statistical post-processing of the same type as described in Section 3.1 could also recover part of the systematic forecast errors.

References

[Aussem 94] A. Aussem, F. Murtagh, M. Sarazin; Dynamical Recurrent Neural Networks and Pattern Recognition Methods for Time Series Prediction: Application to Seeing and Temperature Forecasting in the Content of ESO's VLT Astronomical Weather Station; *Vistas in Astronomy*, **38**, 357–374, 1994.

[Bougeault 95] P. Bougeault, Chen De Hui, B. Fleury, J. Laurent, Investigation of seeing by means of an atmospheric mesoscale numerical simulation, *Appl. Opt.*, **34**, 3481–3488, 1995.

[Erasmus 97] A. Erasmus, R. Peterson; The Feasibility of Forecasting Cirrus Cloud Cover and Water Vapour above Telescope Sites in Northern Chile; *PASP* **109**: 208–214, February 1997.

[CRS4 97] R. Deidda, M. Marrocu, A. Speranza; Feasibility Study of a Meteorological Prediction Model for ESO Observatories In Chile; *VLT Technical Report CRS-17443–0002*, Apr. 1997.

[Masciadri 97] E. Masciadri, J. Vernin, P. Bougeault; Feasibility Study of Seeing Prevision using the MESO-NH meteorological model: a progress report; *VLT Technical Report UNI-17400–0003*; March 1997.

Marc Sarazin
msarazin@eso.org

***SUNSET ON PARANAL**. This photograph, recently taken on Paranal, shows that the VLT is taking shape.*